Human Arm-and-Hand Dynamics Model with Variability Analyses for a Stylus-based Haptic Interface

Michael J. Fu, *Member, IEEE,* M. Cenk Çavuşoğlu , *Senior Member, IEEE*

***Abstract*—Haptic interface research benefits from accurate human arm models for control, and system design. The literature contains many human arm dynamics models, but lacks detailed variability analyses. Without accurate measurements, variability is modeled in a very conservative manner, leading to less than optimal controller and system designs. This paper not only presents models for human arm dynamics, but also develops inter and intra-subject variability models for a stylus-based haptic device. Data from 15 human subjects (9 male, 6 female, ages 20–32) were collected using a Phantom Premium 1.5a haptic device for system identification. In this work, grip force dependent models were identified for 1–3 N grip forces in the 3 spatial axes. Also, variability due to human subjects and grip force variation were modeled as both structured and unstructured uncertainty. For both forms of variability, the maximum variation, 95%, and 67% confidence interval limits were examined. All models were in the frequency domain with force as input and position as output. The identified models enable precise controllers targeted to a subset of possible human operator dynamics.**

***Index Terms*—Haptics and Haptic Interfaces, Physical Human-Robot Interaction Human Operator Modeling, and System Identification.**

I. Introduction

HAPTIC interfaces provide a human operator bilateral force interaction with a remote or virtual environment. The human arm, with its countless configurations and a multitude of applications, is by far the most complex and variable element in haptic interface systems. In order to develop a stable and useful haptic interface, accurate and relevant models of human arm dynamics are a necessity. They are critical for proper stability analysis, interface design, and improving haptic fidelity. However, because the human arm is so dexterous and reconfigurable, researchers have reported that small variations in arm configurations, grip forces, and application environments result in the arm exhibiting a wide range of dynamic behavior [1], [2], [3], [4]. Since the arm's configuration is constantly subjected to slight changes during a haptic manipulation task, this implies that in addition to accurate, task and orientation-dependant models of human arm dynamics, researchers can also benefit from precise information on the variability of those dynamics during haptic manipulation. Without accurate arm dynamics variability models, haptic interface systems are conservatively designed to account for a larger set of variability than sometimes necessary [5]. In contrast, the availability of precise variability measurements will enable more efficient and higher-performance haptic interface systems targeted at subsets of possible human operator dynamics.

Therefore, the current study aimed to not only create models of the arm and hand dynamics, but also study the inter and intra-subject variability observed in the dynamics and model parameters.

Haptic interfaces with a stylus handle were selected as the focus of this work because of their accessibility and relevance to many haptic manipulation tasks. Stylus handles are commonly found on commercially available haptic devices and are convenient for mimicking other tools that require a similar grasping style. Paintbrushes, dentistry tools, and surgical blades are just a few examples of objects that are held in a pinched-grasp similar to how one would hold a stylus.

The models developed in this study used the common convention of force at the hand as the model input and measured hand position as model output because a key capability of haptic devices is the ability to apply forces to the arm and track hand position. This formulation was consistent with the impedance model for human interaction and the two-port framework for haptic interfaces [6], [7].

Dynamic models for the human arm originated with researchers investigating the body's biomechanics, joint dynamics, and mechanical impedance modeling [8], [9], [10], [11], [12]. As robotics and haptic technology became more mature, researchers began to develop single-input-single-output (SISO) models based on mass-spring-dampers (MSD) systems, which have been shown to accurately reflect arm dynamics and are more suitable for real-time computer implementation [13], [14], [15], [11]. More recently, human arm dynamics have been increasingly modeled using robots or manipulators that can be used for haptic feedback in an effort to improve haptic system design and fidelity. For instance, Hasser *et al.* developed a hand grasping model while operating a haptic knob [16]. Woo *et al.* characterized the inertia, stiffness, and viscosity of the arm exerting forces of 0–20 N using a one degree-of-freedom (1 DOF) haptic device [17]. Dong *et al.* described non-parametric frequency responses of human fingers using various grip configurations subjected to a random vibration [18]. Various others have modeled intrinsic and reflexive muscle parameters for the shoulder, elbow, and wrist joints using a 2D (horizontal plane) planar haptic device

Michael J. Fu (mfu@fes.org) is with the Cleveland FES Center of Excellence, LSCDVA Medical Center, Cleveland, OH, USA and M. C. Çavuşoğlu (cavusoglu@case.edu) is with Case Western Reserve University, Cleveland, OH, USA. This paper was submitted in part to the 2010 IEEE Int'l Conf. on Robotics and Automation in Anchorage, Alaska. This work was supported in part by NSF grant CNS-0423253, IIS-0805495, and IIS-0905344.

with a cylindrical grip handle [19], [20], [11]. Speich *et al.* characterized human arm parameters using a 1 DOF haptic device with a spherical handle and also a custom 3 DOF haptic device with a stylus handle [21]. Kuchenbecker *et al.* also used a stylus handle with a grip force sensor on a custom 1 DOF manipulator to characterize the hand and wrist [2].

Researchers have also made progress investigating the vibro-tactile responses of the human hand using haptic devices. McMahan *et al.* identified a five-parameter MSD model of the hand interfaced with a stylus grip haptic device using a 1 DOF linear actuator custom-mounted onto the Phantom's stylus itself (for high frequency 10-200 Hz vibro-tactile feedback applications) [22]. Israr *et al.* have used both stylus-based devices and spherical actuators to shake the hand at 10-500 Hz [23], [24]. Also, Diaz *et al.* have investigated the vibration modes from 0.7–200 Hz in 1 DOF of the human operator using a racquet grip on the Phantom Premium 1.0 and a custom haptic interface [25].

The mentioned works have contributed greatly to haptics research, but what is currently not found in the literature are experimentally-derived results describing the uncertainty and variation found in human arm dynamics. Human operator variability is frequently modeled as the set of all passive nonlinear impedances [26]. However, this approach typically results in overconservative designs, which limit the haptic interface system's performance. More limited uncertainty sets are used in some studies (e.g. [27]), however these models are not based on detailed human experiments. Indeed, many studies used human experiments and reported the amount of variance observed from their data collections and parameter identifications, but the variances are not modeled in a way that can be directly used for robust stability and performance analysis.

Study Objectives

The current work focuses on modeling not only the 3D arm dynamics, but also the inter and intra-subject variability (due to human variation and grip force changes, respectively) as a function of frequency.

This study used data collected from human experiments to identify both grip-force-dependent 3D Cartesian-space models of the human arm and inter-subject variation using force as the model input and measured position as output. The measured human experiment dynamics were modeled using five-parameter linear transfer functions based on the dynamics of one mass, two springs, and two dampers.

Variability of the dynamics was studied in two forms: as the statistics of the identified arm dynamics model parameters (referred to from here on as 'structured variability') and as multiplicative unstructured uncertainty (referred to as 'unstructured variability'). The unstructured variability was modeled in a form consistent with robust stability theory using transfer functions composed of up to five stable complex-conjugate pairs of poles and up to five minimum-phase complex-conjugate pairs of zeros. In this way, they can be directly applied to robust stability analysis of haptic interfaces. The structured variability, on the other hand, is consistent and applicable to mu-synthesis stability analysis methods. Details for robust stability analysis can be found in texts such as [28].

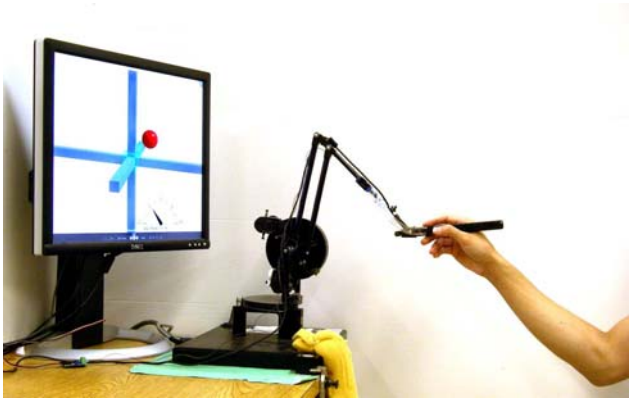

Fig. 1. The experimental setup and arm configuration used for the human experiment data collections.

The arm dynamics and unstructured variability model structures were proposed by the authors in [29], but only nine grip-force-dependent measured-dynamics models and three maximum unstructured variability models were studied. Also, the data in the previous study was collected from nine subjects without the use of stereographic user interface display, or a force sensor at the haptic device end effector. In the current paper, 15 subjects were studied, the user interface was displayed using stereographic 3D images and a force sensor was used for data collection. In addition, structured variability results are introduced along with additional unstructured variability models. Structured variability results were obtained from 135 new measured-dynamics models, one for each axis, subject, and grip force combination. Also, in addition to the maximum observed inter and intra-subject variability, the 95% and 67% confidence interval (CI) limits for variability were also identified and studied.

II. METHODS

The following methods were consistently applied to each of the three Cartesian axes.

A. Subjects

Fifteen subjects (6 female, 9 male, ages 20–32) were recruited with prior consent for this study and were not compensated for their participation. Each subject was free from any movement impairments that would have affected this study and tested using their dominant arm. The experimental procedures were reviewed and given exemption status by the institution's Internal Review Board.

B. Equipment

Experiments were performed using a Phantom Premium 1.5a haptic device (Sensable Technologies Corp., Woburn, MA) equipped with both a Nano 17 6-DOF force/torque sensor (ATI Industrial Automation, Apex, NC) to measure end effector forces and a FlexiForce force-sensitive resistor to measure grip forces (TekScan Corp., Boston, MA). The

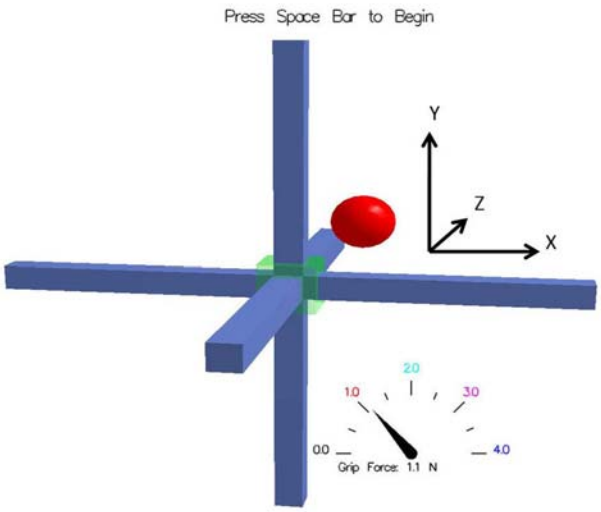

Fig. 2. This was the on-screen view seen by the subjects. The blue cross bars give the user a fixed coordinate frame to judge 3D motion. The sphere is a cursor controlled by moving the haptic device's stylus. The color of the sphere changes to correspond to the label used for each grip force in the gauge located in the lower right of the screen. The green transparent box at the intersection of the crossbars was the static target position each subject was instructed to keep the cursor at during the experiment.

force/torque sensor was attached to the Phantom at the end effector. A custom stylus made of Delrin was attached via the Phantom's stock passive gimbal to the force/torque sensor. The stylus and gimbal together had a mass of 52 g. The grip force sensor was mounted to the surface of the stylus 4 cm from the gimbal's center and a Phidgets Inc. (Calgary, Alberta, Canada) 1018 analog-to-digital interface was used to acquire data from the grip force sensor at 65 Hz. A dual-core 2.53 GHz Xenon workstation (Dell Corp., Round Rock, TX) ran a real-time servo loop of 1 kHz and acquired data from the motor encoders using a PCI-6602 counter and the force sensor using a PCI-6031 analog-to-digital converter (National Instruments Corp., Austin, TX). Motor outputs were controlled using a PCI-DDA08/12 digital-to-analog converter (Measurement Computing Corp., Norton, MA). The user interface was programmed in OpenGL and displayed stereoscopically using a 120 Hz, 22 in CRT monitor (Dell Corp., Round Rock, TX) and Crystal Eyes 3 active shutter glasses (RealD Corp., Beverly Hills, CA).

C. Arm Model Experiment Paradigm

During each experiment trial, the subject was instructed to wear stereographic shutter glasses, sit facing a 22" computer monitor in a chair with no arm rests, and use their hand to hold a stylus-shaped handle at the end effector of the Phantom haptic device as one would hold a pen. Figure 1 shows the arm configuration and experiment setup for the experiments. Since the elbow and wrists were not supported, some muscle contractions (including the biceps, deltoid, and pectoralis major) were required to counter gravity and maintain a fixed hand position. Figure 2 shows the graphical user interface (GUI) presented to the subject. The stereographic GUI displays a spheroid cursor that reflects the motion of the stylus at the gimbal pivot point on a 1:1 scale in virtual 3D space. Each subject's grip force was displayed in two ways: using a gauge and by changing the color of the sphere to signal that a certain grip force was achieved (red for 1 N, cyan for 2 N, and magenta for 3 N). Changing the color of the cursor with respect to the grip force minimizes the need for subjects to divert their attention away from the cursor to the force gauge.

Using the stereographic GUI and the Phantom stylus, the subject was instructed to maintain one of the three tested grip forces (1, 2, and 3 N) and try their best to keep the cursor (red sphere in Fig. 2) at the static target at the center of the crossbars (inside the transparent green box shown in Fig. 2) throughout the duration of the trial. Maintaining a static hand position served to stabilize the hand about the center of the haptic device workspace and minimize any complex cognitive strategies so that the observed dynamics would be largely the result of low-level motor control. Once the subject achieved the desired grip force and centered the cursor at the target, they vocally signaled an experimenter to initiate stimulation forces to the hand along one of the three tested Cartesian coordinate axes. The unstimulated axes of the phantom were unrestrained. When each trial was over, the subject was given as much time as needed to rest and prevent fatigue to their hand and arm caused by the trial. To minimize any order effects, the combinations of grip force and stimulation direction were presented in random order to each subject.

During the experiments, the position at the stylus gimbal's center was recorded in all three degrees of movement (X being left and right, Y being up and down, and Z being forward and backward) while the subject's arm was stimulated with random forces in only one of the degrees of movement at a time (see Sec. II-D). The duration of stimulation lasted 60 s, and the ability of the subject to consistently maintain a specific grip force was monitored by the experimenter via the experiment visual interface described in Sec. II-C. In order not to exceed the 3 A current limit on the Phantom's motors, the stimulation forces at the stylus were limited to not exceed 5 N. Nine sets of data were collected from each subject, one for every combination of three grip forces and three directions of force stimulation (X, Y, and Z directions). The grip forces were the source of inter and intra-subject variability and selected to be 1–3 N because grip forces less than 1 N were insufficient for maintaining a hold on the stylus under the stimulation forces and grip forces greater than 3 N were very difficult for the subjects to consistently maintain for longer than 60 s. Subjects were instructed to maintain a static cursor position at the center of the crossbars in order to trigger a consistent motor control strategy throughout the experiments.

A total of 135 trials were recorded for this study from 15 subjects, three grip forces, and three stimulation axes.

D. Input Signals Used in the Human Experiment

For system identification, input signals such as frequency sweeps, pseudo-random binary sequences, discrete sinusoidal signals, and random noise typically produce comparable results [30], [31]. However, when modeling the human arm, frequency sweeps and discrete sine waves are not suitable

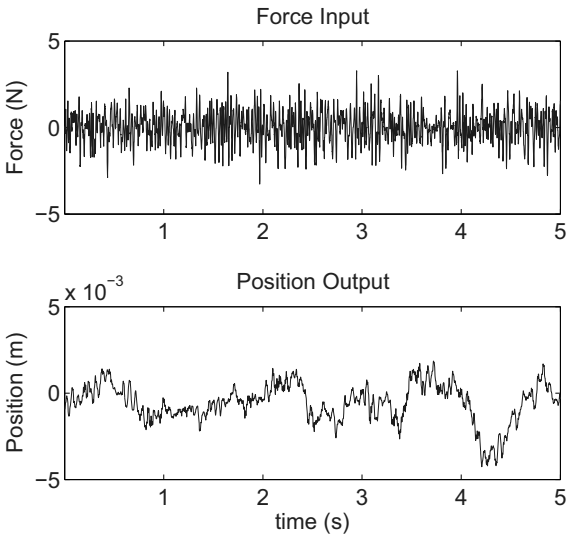

Fig. 3. Example of input and output signals (5 second duration).

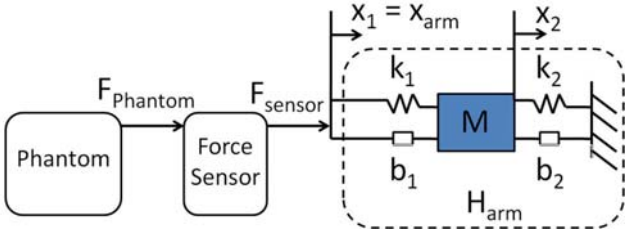

Fig. 4. This block diagram represents the identified system. The left most block represents the haptic device that exerts a force on the human arm. A force sensor (center block) was placed between the haptic device and the user's arm. The dashed box on the right contains the MSD model for the human arm. Mass M represents the inertia of the of the arm. The spring k_1 and damper b_1 represent the hand grasp stiffness while spring k_2 and damper b_2 represent the arm stiffness. $F_{Phantom}$ is the measured force applied at the end effector of the haptic interface and x_{arm} is the measured position of the stylus gimbal center that is attached to the force sensor.

because at low frequencies ($<$ 3 Hz), human anticipatory reflexes make it difficult to keep the arm passive to force disturbances. Fortunately, the more random the force disturbance is, the less likely it will trigger the arm's reflexes. For this reason, the current study used colored noise inputs with a bandwidth of 30 Hz to render them unpredictable by the human subjects and still achieve frequency responses in the range of 0.6–30 Hz. Colored noise was generated from Gaussian white noise that was low-pass filtered to 30 Hz (13th order Butterworth) because of the limits imposed by neural signal delay for voluntary movement (Fig. 3). During complex tasks, such as target reaching, humans take up to 110 ms to respond to changes in target position [32]. It takes approximately 75 ms for a neural signal to travel from the brain to the ankle muscles and back [33]. For the wrist, [34] found that it takes approximately 50 ms to resist an extension by an external force. Since the arm is closer to the brain than the ankle and the target in this study is static, 50 ms was assumed as the approximate time delay for the arm in the experimental task. Under this assumption, the bandwidth for the human arm was approximated to 20 Hz, justifying the selection of 30 Hz noise bandwidth. It is important to note that the current study does not model the neural delay, but serves to provide an approximation for the bandwidth of volitional human movement.

E. Arm Dynamics Model Structure

Figure 4 represents the system that was identified. The human arm was conceptualized as a MSD model containing five parameters (1 mass, 2 springs, and 2 dampers), similar to those used in [35], [21], [36], [25]. In addition to being consistent with models from the literature, MSD models can be readily simulated in real time with common computer hardware and are appropriate for the purposes of the current study's focus on the dynamics at the end-effector of the human arm. Mass M represents the inertia from the arm, spring k_1 and damper b_1 represents the grasp stiffness while spring k_2 and damper b_2 represent the arm stiffness.

A transfer function model for the arm, $H_{\rm arm}$, was then derived (detailed in the Appendix) from the five-parameter MSD model with measured force $F_{\rm sensor}$ as input and position of the hand $X_{\rm arm}$ (considered equal to the measured stylus gimbal center) as output. In Laplace notation, the transfer function (derived in the appendix and consistent with [36], [21]) was

$$H_{\rm arm}(s) = \frac{X_{\rm arm}(s)}{F_{\rm sensor}(s)} = \frac{Ms^2 + (b_1 + b_2)s + k_1 + k_2}{b_1 M s^3 + (b_1 b_2 + k_1 M)s^2 + (b_2 k_1 + b_1 k_2)s + k_1 k_2}, \quad (1)$$

This arm model transfer function was fitted to the measured human experiment frequency response in each axis in order to identify five parameters M, k_1, k_2, b_1, and b_2. The measured human experiment frequency response (arm position as output and force sensor measured force as input) was computed using Welch's transfer function estimation (Matlab's `tfestimate.m`) with 32 Hamming windowed segments and 50% overlap in order to minimize FFT artifacts. Each fit was performed using nonlinear constrained optimization (Matlab `fmincon.m` function) in the frequency domain by minimizing the cost function

$$\sum_{n=1}^{p} W_t(n)\big(H_{\rm exp}(j2\pi\frac{n}{N}) - H_{\rm arm}(j2\pi\frac{n}{N})\big)^2, \quad (2)$$

where $W_t(n)$ was a weighting function, $H_{\rm exp}(s)$ was the frequency response of the force-input, position-output human experiment data, $H_{\rm arm}(s)$ was the measured-dynamics model's frequency response calculated from (1) with the identified parameters, $p = 57$ was the number of data points for 30 Hz of data, and $N = 958$ was the total number of frequency response points resulting from the 32 segment Welch frequency response estimation method. The weighting function, when used, was defined as the mean-squared coherence of the force input and position output, as in [20]. Coherence was calculated via Matlab's `mscohere.m` function with 958 FFT samples to

match the frequency response data. In effect, each empirical frequency response sample was weighted by how closely the input and output signals corresponded at that frequency.

Equation (2) was used as the cost function to identify three sets of arm model structure parameters.

1) Set 1: Grip-Force-Dependent Measured-Dynamics Model Parameters: Parameters for this set were derived from nine measured-dynamics model fits. One model fit was identified for each grip force at each axis. For this set, $H_{\text{exp}}(s)$ was defined as the measured frequency response data averaged over all subjects, resulting in nine grip-force-dependent measured-dynamics model transfer functions. The weighting function used for each fit was the mean-squared coherence averaged over all subjects (Fig. 5). These models provide dynamic equations that are useful for simulating the arm's dynamics during haptic system design.

2) Set 2: Nominal Arm Model Parameters: Parameters in this set were derived from three measured-dynamics model fits, one for each axis. These fits were obtained by defining $H_{\text{exp}}(s)$ as the central complex value of the minimum circle bounding the complex measured frequency response data (real and imaginary values considered to be on orthogonal axes) for all subjects and all grip forces at each frequency sample. The minimum bounding circle center (found using the Crystal-Peirce algorithm in [37]) was necessary in order to find what was effectively the center frequency response of the range at each frequency sample about which variability could be estimated. No weighting function was used for these fits because these models were used to calculate unstructured variability (Sec. II-G).

3) Set 3: Individual Arm Model Parameters: This set was derived from 135 measured-dynamics model fits, one for each subject, grip force, and axis combination. For this set, H_{exp}(s) was defined as each of the 135 total sets of measured frequency response data. The weighting function used for these fits was the mean-squared coherence for each set of the 135 experiments. These parameters were used to calculate the structured variability statistics presented in Sec. II-F).

F. Structured Variability

'Structured variability' refers to the statistical characteristics of the five identified arm model parameters M, k_1, k_2, b_1, and b_2. Structured variability results were obtained from 135 measured-dynamics models using the arm model structure and methods described in Sec. II-E3. From these models, the following statistics were computed: standard deviation, mean, minimum, maximum, and the 95%, and 67% confidence intervals.

G. Unstructured Variability Model

'Unstructured variability' refers to the inter and intra-subject variability observed in the measured arm frequency response, defined as $H^{\text{exp}}_{\text{arm}}(s)$ with respect to the three $\hat{H}_{\text{arm}}(s)$ nominal arm models (Sec. II-E2).

Variability was considered as unstructured multiplicative uncertainty. Under this assumption, the uncertainty model was defined as follows [28].

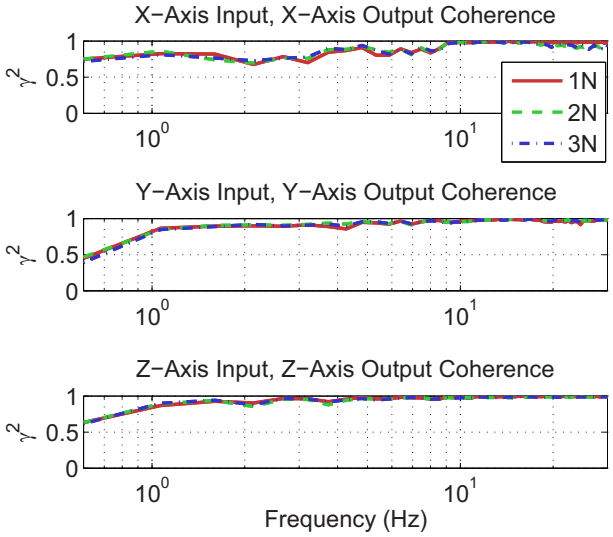

Fig. 5. Subject-averaged mean-squared coherence with force as input and position as output.

For a system with plant transfer function P,

$$P(j\omega) \in \{\hat{P}(j\omega)\big(1 + W_u(j\omega)\Delta(j\omega)\big) : sup|\Delta(j\omega)| \leq 1\}, \quad \Delta(j\omega) \in \mathcal{R} \tag{3}$$

where $\hat{P}$ is the nominal plant transfer function, $W_u(j\omega)$ is the uncertainty weighting function, and $\mathcal{R}$ is the set of all proper real rational functions [28]. The uncertainty weighting function $W_u(j\omega)$ has the relationship

$$|W_u(j\omega)\Delta(j\omega)| \geq |\tfrac{P(j\omega)}{\hat{P}(j\omega)} - 1| \tag{4}$$

and can be interpreted as the percentage uncertainty in the nominal plant $\hat{P}(j\omega)$ at frequency ω.

Therefore, the magnitude of the unstructured uncertainty function $|W_u(j\omega)|$ was considered to represent the unstructured variability of the measured frequency response with respect to the nominal arm models. This was done by using the right side of (4) and defining the nominal arm models, $\hat{H}_{\text{arm}}(s)$, as the nominal plant transfer function $\hat{P}(j\omega)$ and the set of all individual measured frequency responses, $H^{\text{exp}}_{\text{arm}}(s)$, as $P(j\omega)$.

For each axis, a stable and minimum-phase transfer function in Laplace notation of the form

$$V(s) = K\frac{\prod_{i=1}^{N_n}(s - z_i)}{\prod_{i=1}^{N_d}(s - p_i)} \tag{5}$$

with a scaling term K, stable poles p_i, numerator order N_n, minimum-phase zeroes z_i, and denominator order N_d was fitted to envelope the maximum $W_u(j\omega)$ over all subjects and all grip forces using the Matlab's `fmincon.m` function. Each transfer function was constrained to have $N_n \leq N_d$ so that the modeled uncertainty would not asymptotically approach zero. The cost function used was

$$\sum_{n=1}^{p} W_t(n)\Big[\big(W_u(j2\pi\frac{n}{N}) - V(j2\pi\frac{n}{N})\big)^2\Big], \tag{6}$$

TABLE I
ARM STRUCTURE PARAMETERS – GRIP FORCE DEPENDENT MODELS

X-axis	M (kg)	k_1 (N/m)	k_2 (N/m)	b_1 (N·s/m)	b_2 (N·s/m)
1N	0.2892	428.4	99.45	2.998	5.802
2N	0.2869	448.6	93.93	2.443	5.698
3N	0.2731	455.5	96.17	2.325	5.629
Y-axis	M (kg)	k_1 (N/m)	k_2 (N/m)	b_1 (N·s/m)	b_2 (N·s/m)
1N	0.4602	469.69	121.8	7.063	5.996
2N	0.3892	625.94	122.2	5.996	6.005
3N	0.4186	671.20	126.0	5.858	6.410
Z-axis	M (kg)	k_1 (N/m)	k_2 (N/m)	b_1 (N·s/m)	b_2 (N·s/m)
1N	0.2115	843.1	323.9	0.7093	19.42
2N	0.2525	868.3	332.8	0.5882	19.90
3N	0.2353	855.1	355.1	0.4925	20.56

TABLE II
NOMINAL ARM MODEL PARAMETERS

Axis	M (kg)	k_1 (N/m)	k_2 (N/m)	b_1 (N·s/m)	b_2 (N·s/m)
X-axis	0.2179	379.5	78.75	1.839	4.645
Y-axis	0.2692	552.4	105.3	3.609	6.430
Z-axis	0.2041	769.9	271.7	0.7764	18.06

where $W_t(n)$ was a weighting function, $V(j\omega)$ was the variability transfer function from (5), $p = 57$ was the total number of frequency samples for 30 Hz of data, and the total number of frequency samples was $N = 958$ due to the 32 segment Welch frequency response estimation method. The weighting function was tuned visually in order to avoid local minimum solutions that did not properly provide a bound for the computed unstructured uncertainty.

The 67% CI limits for unstructured variability were also examined in order to provide less conservative models for stability analysis. The 67% CI limits were computed using empirically estimated cumulative distribution functions gathered from the experimental data (Matlab's `ecdf.m` function).

III. MEASURED-DYNAMICS MODEL RESULTS

A. Arm Dynamics Model Identification Results

Three sets of arm dynamics models were identified, each with force as input and position as output (Sec. II-E1–II-E3). This paper presents the parameters from Sets 1 and 2, and (for conciseness) only the statistics from Set 3 (consisting of 135 model fits) are presented in Sec. III-B1.

Set 1 consists of nine measured-dynamics models, whose arm structure parameters are listed in Table I. Bode plots for these model transfer functions are shown in Fig. 6.

Parameter Set 2 consisted of three nominal arm models, one representing the center of the range of measured frequency responses for each axis over all grip forces and all subjects. These models were used for the calculation of the unstructured variability models in Sec. II-G. The identified parameters for the nominal arm models are reported in Table II and the Bode plots for the model transfer functions are in Fig. 7a–c.

Each model was identified to accurately reflect the measured frequency response data across 0.6–30 Hz.

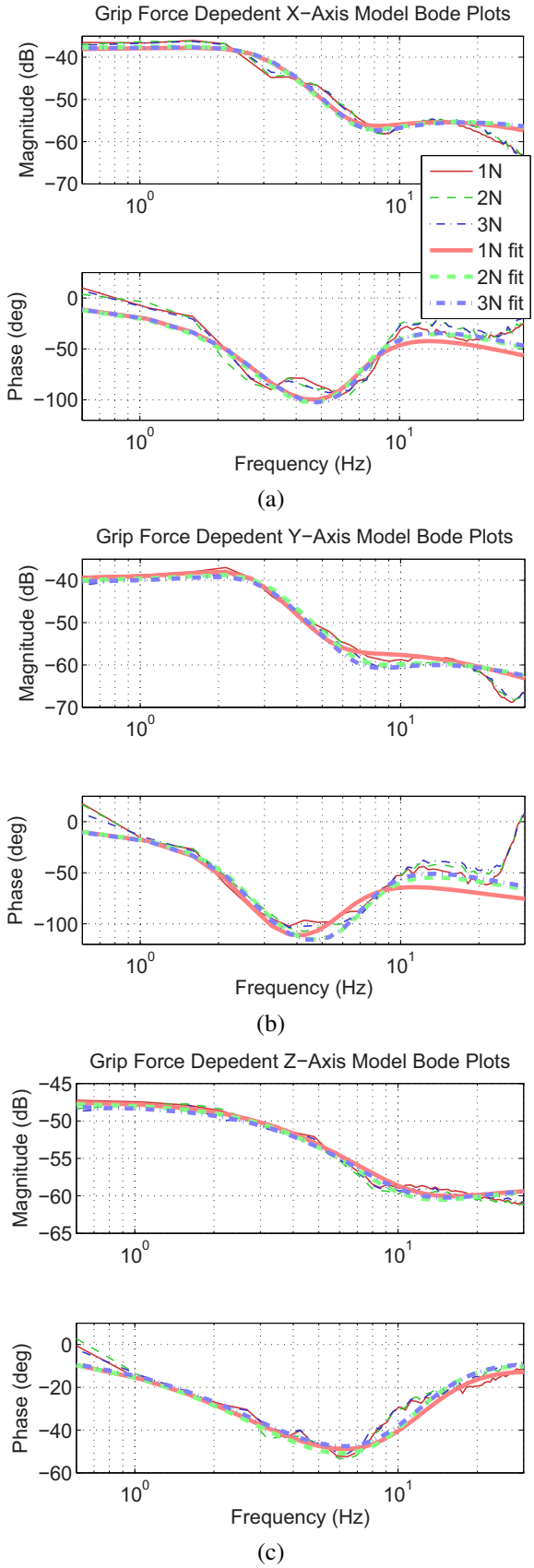

Fig. 6. A–C) The thicker lines are the frequency responses of the grip-force dependent X, Y, and Z-axis measured-dynamics models calculated using (1). The thinner lines are the frequency response of the measured arm dynamics. The model parameters for the 1, 2, and 3 N models are in Table I.

TABLE III
STRUCTURED VARIABILITY - ARM STRUCTURE PARAMETER STATISTICS

X-axis	M (kg)	k_1 (N/m)	k_2 (N/m)	b_1 (N·s/m)	b_2 (N·s/m)
Minimum	0.0340	140.6	53.05	0.0020	3.148
Mean	0.3240	459.4	104.8	2.579	5.920
Maximum	0.8016	757.9	196.2	7.095	10.34
Std Dev	0.1464	144.5	27.59	1.337	2.192
95% CI Min	0.1433	228.0	63.20	0.8686	3.678
95% CI Max	0.5664	650.5	151.3	4.561	10.29
67% CI Min	0.2527	393.0	91.12	1.957	4.372
67% CI Max	0.3759	539.6	116.8	2.883	6.222
Y-axis	M (kg)	k_1 (N/m)	k_2 (N/m)	b_1 (N·s/m)	b_2 (N·s/m)
Minimum	0.2275	292.3	88.66	3.830	4.020
Mean	0.4763	620.2	132.5	6.094	5.890
Maximum	0.9115	926.5	199.7	9.898	9.721
Std Dev	0.1528	185.8	29.05	1.403	1.398
95% CI Min	0.2747	313.1	90.10	4.212	4.145
95% CI Max	0.7221	896.6	194.7	8.904	8.591
67% CI Min	0.3852	525.1	115.5	5.304	5.150
67% CI Max	0.5367	738.6	144.7	6.425	6.272
Z-axis	M (kg)	k_1 (N/m)	k_2 (N/m)	b_1 (N·s/m)	b_2 (N·s/m)
Minimum	0.0003	590.3	194.6	0.0002	10.66
Mean	0.2357	886.9	365.8	0.5241	20.14
Maximum	0.4810	1050	588.7	1.939	28.88
Std Dev	0.1261	105.4	105.8	0.4884	5.129
95% CI Min	0.0161	679.1	214.1	0.0002	13.09
95% CI Max	0.4252	1043	533.0	1.420	27.61
67% CI Min	0.1630	849.4	293.3	0.1091	16.28
67% CI Max	0.2968	941.0	421.6	0.8081	24.67

B. Variability Results

The observed inter and intra-subject arm dynamics variability across all subjects and grip forces was identified in two forms: structured variability and unstructured variability.

1) Structured Variability: Structured variability was characterized across all subjects and grip forces using statistics from 135 individual arm dynamic model fits. For the sake of conciseness, the actual model parameters were not reported, but their statistics are reported in Table III. The root-mean-squared error between the measured position and model-simulated position outputs for all 135 models was found to have an average of 2.39 mm with a standard deviation of 2.73 mm (7.25 mm maximum and 0.72 mm minimum).

2) Unstructured Variability: For the unstructured variability models, multiplicative unstructured uncertainty was calculated using the nominal arm models (Table II) and (4). Force conciseness, the maximum and 67% CI data were reported and not the 95% CI data, as the 95% CI data differed by less than 5 dB from the maximum uncertainty in the 0.6–30 Hz frequency range. Each unstructured variability model was a transfer function consisting of up to five stable complex-conjugate pole pairs and five minimum-phase complex-conjugate zero pairs. Table IV reports the poles and zeros for the transfer functions as fitted for the maximum and 67% CI limits. Each unstructured variability model closely enveloped the uncertainty observed from all 16 subjects and 1–3N grip forces from 0.6–30 Hz, as seen in Fig. 7d–f.

The maximum unstructured uncertainty observed for all three axes was $<$ 10 dB from 0.6–30 Hz. In the same frequency range, the the 67% CI variability models were all $<$ 0 dB and exhibited approximately 10 dB less multiplicative uncertainty than the maximum uncertainty.

TABLE IV
UNSTRUCTURED VARIABILITY MODEL POLES AND ZEROES

X-Axis	Max Variance	67% Confidence Interval
K	1.322	0.4476
Zero Pair 1	$-3.420 \pm 12.88j$	$-68.65 \pm 0.000j$
Zero Pair 2	$-67.28 \pm 0.0024j$	$-2.349 \pm 7.134j$
Zero Pair 3	$-2.714 \pm 6.183j$	$-54.65 \pm 133.3j$
Zero Pair 4	$-5.458 \pm 27.34j$	$-6.627 \pm 41.04j$
Zero Pair 5	$-29.81 \pm 159.5j$	–
Pole Pair 1	$-2.294 \pm 4.224j$	$-41.16 \pm 0.0011j$
Pole Pair 2	$-53.48 \pm 69.71j$	$-8.028 \pm 42.57j$
Pole Pair 3	$-54.64 \pm 160.1j$	$-4.297 \pm 7.713j$
Pole Pair 4	$-1.971 \pm 13.26j$	$-43.17 \pm 167.8j$
Pole Pair 5	$-4.536 \pm 27.25j$	–
Y-Axis	Max Variance	67% Confidence Interval
K	1.856	1.163
Zero Pair 1	$-2.259 \pm 7.250j$	$-2.379 \pm 8.072j$
Zero Pair 2	$-23.53 \pm 129.2j$	$-10.43 \pm 18.00j$
Zero Pair 3	$-6.371 \pm 39.57j$	$-43.20 \pm 99.69j$
Zero Pair 4	$-16.45 \pm 92.46j$	$-1547 \pm 331.6j$
Zero Pair 5	$-5.785 \pm 30.96j$	–
Pole Pair 1	$-56.82 \pm 66.53j$	$-93.89 \pm 128.0j$
Pole Pair 2	$-19.90 \pm 49.73j$	$-8.189 \pm 0.000j$
Pole Pair 3	$-3.334 \pm 4.181j$	$-756.9 \pm 1363j$
Pole Pair 4	$-19.81 \pm 117.5j$	$-6.038 \pm 15.00j$
Pole Pair 5	$-2.908 \pm 34.03j$	–
Z-Axis	Max Variance	67% Confidence Interval
K	2.592	0.5320
Zero Pair 1	$-1.312 \pm 6.482j$	$-924.6 \pm 122.0j$
Zero Pair 2	$-208.8 \pm 0.5379j$	$-40.12 \pm 84.57j$
Zero Pair 3	$-20.09 \pm 38.93j$	$-1.842 \pm 6.803j$
Zero Pair 4	$-5.210 \pm 19.61j$	$-10.63 \pm 39.00j$
Zero Pair 5	$-5.004 \pm 40.79j$	$-6.796 \pm 95.29j$
Pole Pair 1	$-388.7 \pm 18.74j$	$-13.19 \pm 44.69j$
Pole Pair 2	$-4.004 \pm 17.33j$	$-2.594 \pm 6.321j$
Pole Pair 3	$-7.647 \pm 49.51j$	$-73.98 \pm 0.0048j$
Pole Pair 4	$-2.042 \pm 6.189j$	$-487.2 \pm 964.86j$
Pole Pair 5	$-5.494 \pm 35.932j$	$-8.092 \pm 95.687j$

IV. DISCUSSION

The proposed arm model structure produced transfer functions that closely matched the frequency response of the measured data from 0.6–30 Hz for the X, Y, and Z axes. As seen in Fig. 6, the model frequency responses best matched empirical data up to 20 Hz for all axes. From 20–30 Hz, however, the differences between the model and empirical frequency responses were more apparent. This may suggest the need for further study to model frequencies beyond 20 Hz, which may be dominated by dynamics outside the scope considered in the current study (such as low-level motor reflexes or other non-linear dynamics). Specific to the higher frequencies, several studies have begun to use MSD models to investigate the hand's vibro-tactile response to force inputs in the ranges between 10-500 Hz [22], [23], [24], [25].

Also, it is important to note that the slight differences between the nominal model and empirical frequency responses between 20–30 Hz (Fig. 7) does not change the validity of the unstructured variability results. This is due to the fact that the unstructured variability bounds are designed to envelope the variation of the empirical frequency response about the nominal model frequency response.

A. Comparison with Previous Arm Model Parameters

The identified models successfully captured the magnitude response plateaus that start around 10 Hz in all three axes

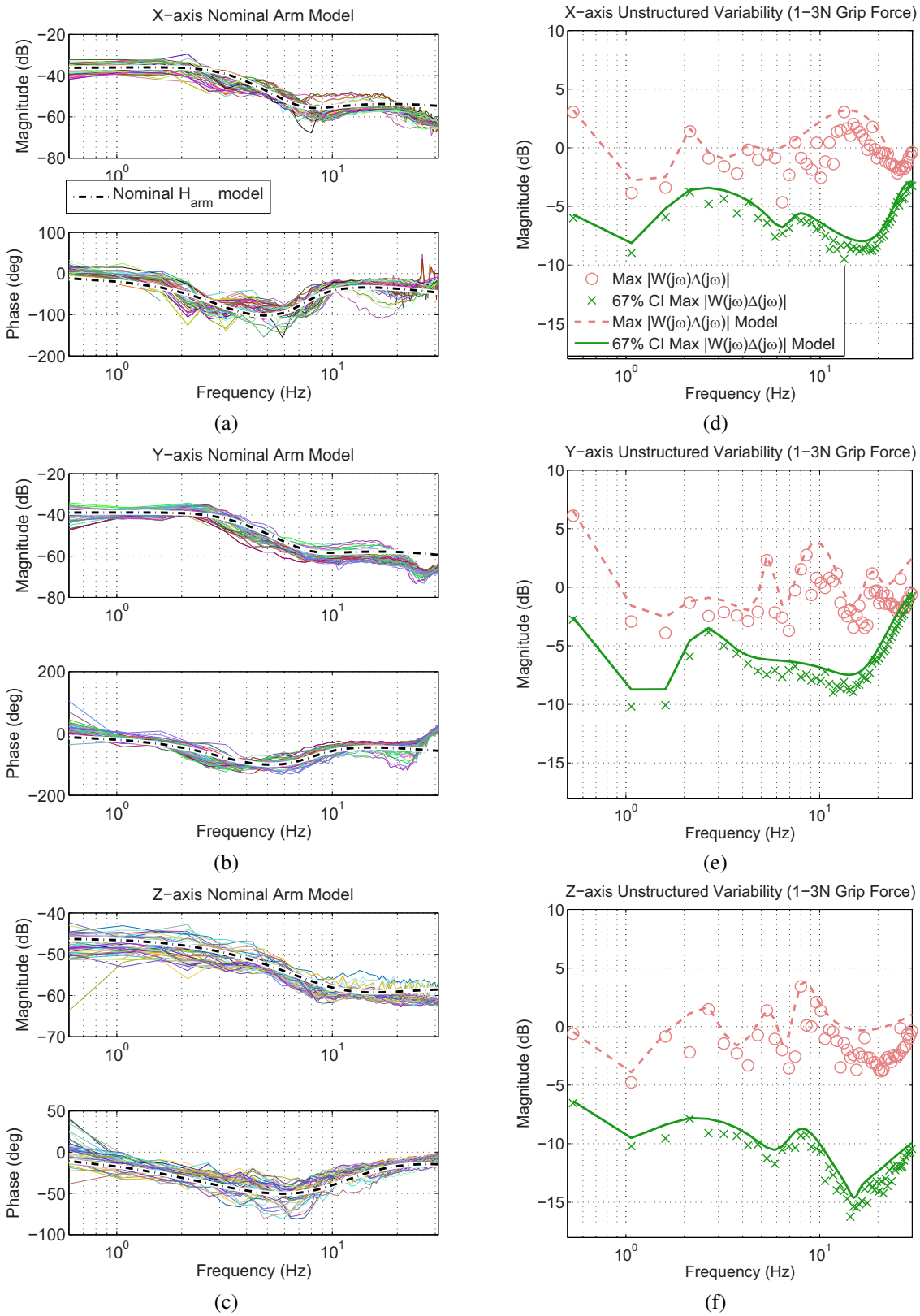

Fig. 7. A–C) For each axis, the black dotted lines representing the nominal arm model $\hat{H}_{\text{arm}}(s)$ Bode plots (whose parameters are in Table II) are plotted over the multi-colored thin lines showing the measured frequency responses for all subjects and all grip forces, $H^{\text{exp}}_{\text{arm}}(s)$. These arm models were used as the nominal model for calculating the unstructured uncertainty in (4). D–F) Magnitude response for the inter/intra-subject unstructured variability models of the X, Y, and Z axes (dashed pink like for the max model and solid green line for 67% model) plotted along with the maximum uncertainty and 67% CI limits they were modeled after (pink x markers and green circles, respectively).

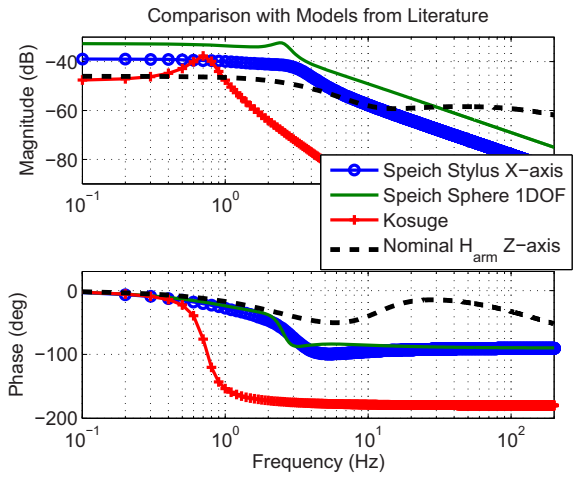

Fig. 8. The frequency responses of different models reported in literature (solid color lines) to the current study's nominal Z-axis arm model (black dashed line). All models correspond to forward and backward motion.

(Fig. 6a–c). Similar behavior in the measured magnitude response was observed in [21], which also modeled the human arm using a 3 DOF stylus-based manipulator. However, their transfer functions were fitted from 0.5–10 Hz and therefore, were not designed to capture the plateau characteristics present in the measured data. As a result, the current model behaves quite differently beyond 10 Hz than past models.

However, up to 10 Hz, the frequency response of the current models are comparable to existing results. Figure 8 shows the current nominal arm Z-axis $\hat{H}_{\rm arm}$ model plotted on the same scale with similar arm models from literature that also modeled forward and backward direction motion. Speich, *et al.* used a five-parameter MSD model with a transfer function similar to (1). Kosuge used a three-parameter model (mass m, spring k, damper b) resulting in a second-order transfer function expressed by

$$H_{arm}(s) = \frac{Position(s)}{Force(s)} = \frac{1}{ms^2 + bs + k}. \qquad (7)$$

Although Kosuge's model structure and experimental methods differ significantly from the current experiment, it is referenced here to represent the frequency response of second order models.

Up to 10 Hz, the current model was most similar in frequency response to Speich, *et al*'s stylus handle model. Their other model used a 1 DOF sphere-handled manipulator, which exhibited a resonant peak at 3 Hz. The other models in Fig. 8 were identified for fidelity in the lower frequency ranges ($<$ 10 Hz), assume a joystick handle grasp, and are second order, so they drop off at 40 dB/dec from 1–2 Hz. In contrast, the current model maintains valuable dynamics that occurred past 10 Hz.

Table V lists model parameters from literature for the models shown in Fig. 8 in addition to identified parameters from [25] and [35]. The magnitude responses for [25] and [35] were not plotted in Fig. 8 because the human operator MSD parameters were coupled and identified along with other dynamics, such as neural delays and manipulator vibration

TABLE V
ARM MODEL PARAMETERS FROM LITERATURE

	M(kg)	k_1(N/m)	k_2(N/m)	b_1(N·s/m)	b_2 (N·s/m)
Diaz [25]	0.22	3662	98.6	1.18	6.88
Speich [21] X	0.85	122	330	12.9	12.9
Speich Y	4.03	108	104	9.20	47.6
Speich Z	0.68	81.4	13.0	17.6	13.5
Speich 1DOF	1.46	48.8	375	4.5	7.9
Vlugt [35]	1.88	14998	733	178	37.3
Kosuge [15]	11.6	–	243	–	17.3

modes. For the five-parameter models from literature, it was assumed that $k_1, b_1 = k_s, b_s$ and $k_2, b_2 = k_h, b_h$ in [25], while $k_1, b_1 = k_h, b_h$ and $k_2, b_2 = k_a, b_a$ in [35]. Also, for the three-parameter arm models, it was assumed that the spring and damper correspond to k_2 and b_2 in the current model structure (implying a rigid link between the hand and the haptic device). Of the cited models, only Speich's X, Y, and Z models identified the hand in a stylus grip configuration; Speich's 1 DOF used a spherical knob, [25] used a horizontal tennis racquet grip and the rest used vertical joystick grip configurations.

It was also observed that the identified parameters of the current model structure were comparable to existing results. The mass parameters of the current models were identified to be between 0.0003–0.91 kg, which overlapped the range of 0.22–11.6 kg in past studies . This study's stiffness results ranged from 141–1050 N/m for k_1 and 53–589 N/m for k_2, which were within the 48.8–14998 N/m for k_1 and 13–733 N/m for k_2 reported in literature. The current results also showed that damping parameters ranged between 0.0002–9.9 N·s/m for b_1 and 3.1–29 N·s/m for b_2, which was lower, but also overlapped the range of 1.18–178 N·s/m for b_1 and 5.5–47.6 N·s/m for b_2 reported by literature.

It is noteworthy that the identified model parameter ranges do not provide bounds on the range of parameters from literature, but this is not unexpected. The current study is relevant for a stylus grasp configuration similar to Fig. 1 while applying 1-3 N grip forces. In contrast, methods from the cited literature differ in significant ways, such as in model structure, grip forces used by subjects, and arm configuration – all of which can affect the arm's response. Thus, since the current variability results were not designed to encompass all those variations, it is possible for the identified parameter ranges to exclude some of those from the literature.

B. Grip-Force-Dependent Models

Some apparent trends were observed from the subject-averaged grip-force-dependent fits (Sec. II-E1 and Table I), but statistical tests for grip-force trends on the 135 individual fits (Sec. II-E3) did not reach statistical significance. Statistical analyses consisted of one-way repeated measures analysis of variance with Greenhouse-Geisser sphericity correction and Holm-Sidak multiple comparison tests (grip force as the factor).

The lack of clear trends was possibly because only three grip forces were examined in this study. A more appropriate

study design for trend analysis will likely require a wider range and more grip force levels. However, due to fatigue concerns during the 60 s of force input, the currently study was able to only test three grip forces.

There were, however, notable differences in the Z-axis spring and damping parameters compared to the other axes (Table I). Specifically, the Z-axis k_1, k_2, and b_2 parameters were increased more than 2 times beyond the range of their counterparts for the X and Y axes, while b_1 was approximately one order of magnitude less. One interpretation of this is that the Z-axis had decreased damping, but higher stiffness near the stylus handle and higher stiffness and damping further away from the stylus. The cause for these parameter discrepancies is not obvious and there is no mention of similar phenomenon in the literature.

However, Z-axis motion kinematics were observed to differ from that of the other axes and could be a contributing factor. For all three axes, since a grip force was maintained, the wrist joint was very rigid compared to the elbow and shoulder joints. Therefore, force inputs to the X (left/right) and Y (up/down) axes predominantly cause rotations about one joint, the shoulder or the elbow, respectively. But Z-axis force stimulation resulted in forward/backward motion that requires both the shoulder and elbow joints. Also, X and Y-axis forces apply torques over the length of the forearm, while Z-axis forces apply torque over the length of the upper arm.

C. Unstructured Variability

As seen in Fig. 7d–f, the proposed unstructured variability structure was successful in producing models that closely enveloped both the maximum and 67% CI limits from the measured data. Also, the unstructured variability models (Table IV) were computationally-simple, minimum-phase and stable transfer functions. These transfer functions can be used to compute multiplicative uncertainty bounds on the nominal arm model transfer functions (Table II).

The developed nominal and variability models can be used in various robust control design and analysis techniques. Specifically, the multiplicative unstructured uncertainty models are used for robust performance and stability in the H-infinity control design framework. Arm models with unstructured uncertainty are constructed, consistent with (3) as

$$H^u_{arm}(s) \in \{\hat{H}_{arm}(s)\big(1 + W_u(s)\Delta(s)\big) : sup|\Delta(s)| \leq 1\}, \quad \Delta(s) \in \mathcal{R} \tag{8}$$

where the nominal arm transfer function $\hat{H}_{arm}(s)$ is (1) with parameters from Table II, unstructured variability $W_u(s)$ is (5) with parameters from Table IV, and $\mathcal{R}$ is the set of all proper real rational functions.

Both the structured and unstructured uncertainty models can be used for controller design using the μ-synthesis framework. Structured Variability models can be used for robust stability analysis using Kharitonov's Theorem [38]. Previous work, which used robust analysis methods that can employ the current models include [39], [40], [27], [41], [42].

It is important to note that the identified uncertainty models are overbounds on the set of transfer function models of the arm dynamics and that the actual variability may only be a smaller subset. Such representations may also lead to somewhat conservative robustness analyses. Specifically, the obtained unstructured multiplicative uncertainty models for the maximum variation case exceeded 0 dB for most of the 0.6–30 Hz frequency range and may lead to conservative results.

D. Limitations

The current experiments and models were designed to be linearized, small-signal approximations centered about a fixed stabilization point and arm configuration. Additionally, the variability captured in the variability models are due to variations caused by grip force changes of 1-3 N and intrasubject and intersubject factors. Therefore, due to the dexterity of the human arm and hand, further study is necessary for arm configurations and grip forces that significantly deviate from that which was investigated. Examples of significant changes include changes in the hand's grasp orientation or supporting the weight of the arm at the elbow or wrist. However, even though the current results are not generalizable, the studied arm configuration is common for dexterous manipulation using commercially-available haptic interface devices.

V. Conclusion

This paper presented models of the arm and hand dynamics based on a five-parameter MSD model. These models are relevant in the context of stylus-based haptic devices operated by the human arm with a configuration similar to that depicted in Fig. 1 for grip forces of 1–3 N. Empirical data from 15 individuals were used to identify both grip-force-dependent and nominal arm models which had identified parameters and frequency responses that were consistent with literature. The models were force-input, position-output transfer functions that were accurate to the measured data in the frequency range of 0.6–30 Hz for the X and Y and Z-axes. Also, the current work presented inter and intra-subject model variability data in the form of both structured and unstructured variability. The structured variability was the computed statistics from 135 individually identified arm dynamics models and the unstructured variability consisted of experimentally-derived transfer functions that accurately modeled the unstructured multiplicative uncertainty found in the X, Y, and Z axes. The structured variability and 67% unstructured variability results were new to literature and provide experimentally-derived uncertainty bounds useful for designing precise controllers targeted to a subset of possible human operator dynamics.

Appendix

Arm Model Transfer Function Derivation

Equation (1) was derived from the MSD model in Fig. 4 as follows in Laplace notation (leaving out the dependency of $F_{\text{sensor}}(s)$, $X_{\text{arm}}(s) = X_1(s)$, and $X_2(s)$ on the Laplace variable s for legibility). First, the differential equation for mass M is transformed into the Laplace domain and $X_2(s)$

was found as

$$\begin{aligned} M\ddot{x_2} &= k_1(x_1 - x_2) + b_1(\dot{x_1} - \dot{x_2}) - k_2 x_2 - b_2\dot{x_2} \\ \overset{\mathscr{L}}{\longleftrightarrow} Ms^2X_2 &= k_1(X_1 - X_2) + b_1 s(X_1 - X_2) - X_2(k_2 + b_2 s) \\ \rightarrow X_2 &= \frac{X_1(k_1 + b_1 s)}{Ms^2 + (b_1 + b_2)s + k_1 + k_2}. \end{aligned} \tag{9}$$

Then, the measured force $F_{\text{sensor}}(s)$ was solved for as

$$\begin{aligned} 0 &= F_{\text{sensor}} - k_1(x_1 - x_2) - b_1(\dot{x_1} - \dot{x_2}) \\ \overset{\mathscr{L}}{\longleftrightarrow} 0 &= F_{\text{sensor}} - k_1(X_1 - X_2) - b_1 s(X_1 - X_2) \\ \rightarrow F_{\text{sensor}} &= X_1(k_1 + b_1 s) - (K_1 + b_1 s)X_2. \end{aligned} \tag{10}$$

Finally, (9) was substituted into (10) to find the transfer function $H_{\text{arm}}(s)$ in (1), with $x_1 = x_{\text{arm}}$.

REFERENCES

[1] H. Gomi, Y. Koike, and K. M., "Human hand stiffness during discrete point-to-point multi-joint movement," *Proc. of the Annual International Conference of the IEEE EMBS*, vol. 14, pp. 1628–1629, October - November 1992.

[2] K. J. Kuchenbecker, J. G. Park, and G. Niemeyer, "Characterizing the human wrist for improved haptic interaction," *Proc. of the 2003 International Mechanical Engineering Congress and Exposition*, pp. 1–8, November 2003.

[3] L. A. Jones and H. I. W., "Influence of the mechanical properties of a manipulandum on human operator dynamics: elastic stiffness," *Biological Cybernetics*, vol. 62, no. 4, pp. 299–307, 1990.

[4] ——, "Influence of the mechanical properties of a manipulandum on human operator dynamics: viscocity," *Biological Cybernetics*, vol. 69, no. 4, pp. 295–303, 1993.

[5] A. Haddadi and K. Hashtrudi-Zaad, "Bounded-Impedance Absolute Stability of Bilateral Teleoperation Control Systems," vol. 3, no. 1, pp. 15–27, January–March 2009.

[6] N. Hogan, "Controlling impedance at the man/machine interface," *Proc. of the IEEE International Conference on Robotics and Automation, Scottsdale, AZ*, vol. 3, pp. 1621–1631, May 1989.

[7] R. J. Adams and B. Hannaford, "A two-port framework for the design of unconditionally stable haptic interfaces," *Proc. of the 1998 IEE/RSJ Int. Conf. on Intelligent Robots and Systems*, pp. 1254–1259, 1998.

[8] J. Winters, L. Stark, and S.-N. A. H., "An analysis of the sources of musculoskeletal system impedance," *Journal of Biomechanics*, vol. 21, no. 12, pp. 1011–1025, 1988.

[9] J. B. MacNeil, R. E. Kearney, and I. W. Hunter, "Time-varying identification of human joint dynamics," *Proc. of the 11th IEEE EMBS Inter. Conf.*, 1989.

[10] C. C. Gielen and J. C. Houk, "Nonlinear viscosity of human wrist," *Journal of Neurophysiology*, vol. 52, no. 3, pp. 553–569, September 1984.

[11] T. Tsuji, K. Goto, M. Moritani, M. Kaneko, and P. Morasso, "Spatial characteristics of human hand impedance in multi-joint arm movements," in *Proceedings of the IEEE International Conference on Intelligent Robots and Systems*, vol. 1, September 1994, pp. 423–430.

[12] R. Gurram, S. Rakheja, and A. J. Brammer, "Driving-point mechanical impedance of the human hand-arm system: Synthesis and model development." *Journal of Sound and Vibrations*, vol. 180, no. 3, pp. 437–458, 1995.

[13] R. E. Kearney and I. W. Hunter, "System identification of human joint dynamics," *Critical Reviews in Biomedical Engineering*, vol. 18, no. 1, pp. 55–87, 1990.

[14] D. A. Lawrence, "Stability and transperancy in bilateral teleoperation," *IEEE/ASME Trans. Mechatronics*, vol. 9, no. 5, pp. 624–637, October 1993.

[15] K. Kosuge, Y. Fujisawa, and F. T., "Control of mechanical system with man-machine interaction," *Proc. of the IEEE/RSJ International Conference on Intelligent Robots and Systems*, pp. 87–92, 1992.

[16] C. J. Hasser and M. R. Cutkosky, "System identification of the human grasping a haptic knob," *Proc. of the 10th Symposium on Haptic Interfaces for Virtual Environment and Teleoperator Systems, Orlando, FL*, pp. 117–180, March 2002.

[17] H. Woo and D. Lee, "Exploitation of the impedance and characteristics of the human arm in the design of haptic interfaces," *IEEE Trans. Ind. Electron.*, vol. 56, no. 9, p. in press, 2009.

[18] R. G. Dong, D. E. Wecome, T. W. McDowell, and T. Z. Wu, "Biodynamic response of human fingers in a power grip subjected to a random vibration," *Journal of Biomechanical Engineering*, vol. 126, pp. 447–457, August 2004.

[19] E. Vlugt and A. C. Schouten, "Identification of intrinsic and reflexive muscle parameters of the human arm in 3d joint space," *Proc. of the 2004 IEEE Int. Conf. on Systems, Man, and Cybernetics*, pp. 2471–2478, 2004.

[20] E. J. Perreault, R. F. Kirsch, and P. E. Crago, "Effects of voluntary force generation on the elastic components of endpoint stiffness," *Experimental Brain Research*, vol. 141, pp. 312–323, 2001.

[21] J. E. Speich, L. Shao, and M. Goldfarb, "Modeling the human hand as it interacts with a telemanipulation system," *Mechatronics*, vol. 15, no. 9, pp. 1127–1142, November 2005.

[22] W. McMahan and K. J. Kuchenbecker, "Haptic display of realistic tool contact via dynamically compensated control of a dedicated actuator." *Proc. of the 2009 IEEE/RSJ Int. Conf. on Intelligent Robots and Systems*, pp. 3170–77, October 2009.

[23] A. Israr, S. Choi, and H. Z. Tan, "Detection threshold and mechanical impedance of the hand in a pen-hold posture." *Proc. of the 2006 IEEE/RSJ Int. Conf. on Intelligent Robots and Systems*, pp. 472–477, 2006.

[24] ——, "Mechanical impedance of the hand holding a spherical tool at threshold and suprathreshold stimulation levels," in *WHC '07: Proceedings of the Second Joint EuroHaptics Conference and Symposium on Haptic Interfaces for Virtual Environment and Teleoperator Systems*. Washington, DC, USA: IEEE Computer Society, 2007, pp. 56–60.

[25] I. Díaz and J. J. Gil, "Influence of vibration modes and human operator on the stability of haptic rendering," *IEEE Trans. Robot.*, vol. 26, no. 1, pp. 160–165, 2010.

[26] G. Niemeyer and J. J. E. Slotine, "Stable adaptive teleoperation," *IEEE Journal of Oceanic Engineering*, vol. 16, no. 1, pp. 152–162, January 1991.

[27] M. C. Çavuşoğlu, A. Sherman, and F. Tendick, "Design of bilateral teleoperation controllers for haptic exploration and telemanipulation of soft environments," *IEEE Trans. Robot.*, vol. 18, no. 4, pp. 641–647, August 2002.

[28] K. Zhou, J. C. Doyle, and K. Glover, *Robust and Optimal Control*. Edgewood Cliffs, NJ: Prentice Hall, 1996.

[29] M. J. Fu and M. C. Çavuşoğlu, "Three-dimensional human arm and hand dynamics and variability model for a stylus-based haptic interface," *Proc. of the 2010 IEEE/RSJ Int. Conf. on Robotics Automation*, pp. 1339–1346, May 2010.

[30] L. Ljung, *System Identification: Theory for the User*, 2nd ed. PTR Prentice-Hall, Upper Saddle River, NJ, 1999.

[31] Y. Xu and J. M. Hollerbach, "Nonlinear Time-Varying Identification of Human Arm Joint Mechanical Properties using a Portable Pneumatic Thruster," in *Proc. of the American Control Conference*, 1997, pp. 3281–85.

[32] E. Brenner and J. B. J. Smeets, "Fast responses of the human hand to changes in target position," *Journal of Motor Behavior*, vol. 29, no. 4, pp. 297–321, December 1997.

[33] R. Shadmehr and S. P. Wise, *The Computational Neurobiology of Reaching and Pointing, A Foundation for Motor Learning*, ser. Computational Neuroscience Series, T. J. Sejnowski and T. A. Poggio, Eds. Cambridge, MA: The MIT Press, 2005.

[34] J. E. Marsden and T. J. R. Hughes, *Mathematical foundations of elasticity*. Englewood Cliffs, NJ, USA: Prentice-Hall, Inc., 1983.

[35] E. de Vlugt, A. C. Schouten, and F. C. van der Helm, "Adaptation of reflexive feedback during arm posture," *Biological Cybernetics*, vol. 87, no. 1, pp. 10–26, 2002.

[36] K. B. Fite, L. Shao, and M. Goldfarb, "Loop shaping for transparency and stability robustness in bilateral telemanipulation," *IEEE Trans. Robot. Autom.*, vol. 20, no. 3, pp. 620–624, 2004.

[37] D. W. Hearn and J. Vijay, "Efficient algorithms for the (weighted) minimum circle problem," *Operations Research*, vol. 30, no. 4, pp. 777–795, 1982.

[38] W. S. Levine, Ed., *The Control Handbook*. Boca Raton, FL: CRC Press LLC, 1996.

[39] H. Kazerooni, T.-I. Tsay, and K. Hollerbach, "A controller design framework for telerobotic systems," *IEEE Trans. Control Syst. Technol.*, vol. 1, no. 1, pp. 50–62, March 1993.

[40] J. Yan and S. E. Salcudean, "Teleoperation controller design using H-infinity optimization with application to motion-scaling," *IEEE Trans. Control Syst. Technol.*, vol. 4, no. 3, pp. 244–258, May 1996.
[41] K. Kim, M. C. Çavuşoğlu, and W. K. Chung, "Quantitative comparison of bilateral teleoperation systems using μ synthesis," *IEEE Trans. Robot.*, vol. 23, no. 4, pp. 776–789, August 2007.
[42] A. Shahdi and S. Sirouspour, "Adaptive/Robust Control for Time-Delay Teleoperation," *IEEE Trans. Robot.*, vol. 25, no. 1, pp. 196–205, Februrary 2009.

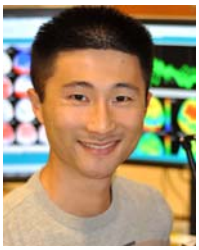

Michael J. Fu (S'06-M'12) is currently a post-doctoral investigator with the Cleveland Functional Electrical Stimulation (FES) Center of Excellence at the Louis Stokes Cleveland Department of Veterans Affairs Medical Center with a joint appointment in the Department of Orthopaedics at MetroHealth Medical Center in Cleveland, OH. In 2007, he was a visiting scholar at the National Aeronautics and Space Administration (NASA) Glenn Research Center.

He received a B.S. degree in electrical engineering and computer science from the University of California, Berkeley in 2003, and the M.S. and Ph.D. degrees in electrical engineering from Case Western Reserve University (CWRU), Cleveland, OH in 2006 and 2011, respectively.

Dr. Fu's research program is centered on the translation of human-computer interface technologies (such as virtual environments, robotics, and functional electrical stimulation) to design novel approaches to motor and cognitive relearning after neural injury. This involves not only new strategies for rehabilitation therapy, but also characterization of human task performance, quantification of injury-related impairment, and investigation into the mechanisms of neural repair. Dr. Fu has and continues to serve as a reviewer for numerous IEEE publications and conferences.

M. Cenk Çavuşoğlu M. Cenk Cavusoglu (S'93-M'01-SM'06) received the B.S. degree in electrical and electronic engineering from the Middle East Technical University, Ankara, Turkey, in 1995, and the M.S. and Ph.D. degrees in electrical engineering and computer sciences from the University of California, Berkeley, in 1997 and 2000, respectively.

He is currently an Associate Professor of Electrical Engineering and Computer Science at Case Western Reserve University, Cleveland, OH. Previously, he was a a Visiting Researcher at the INRIA Rhones-Alpes Research Center, France (1998), a Postdoctoral Researcher and Lecturer at the University of California, Berkeley (2000-2002), and a Visiting Associate Professor at the Bilkent University, Ankara, Turkey (2009-2010).

Dr. Cavusoglu's research involves applications of robotics and control engineering to biomedical and biologically-inspired engineered systems. Specifically, his research interests include robotics, systems and control theory, and human-machine interfaces, with emphasis on Medical Robotics, Haptics, Virtual Environments, Surgical Simulation, and Bio-System Modeling and Simulation. Dr. Cavusoglu has served as an Associate Editor of the IEEE TRANSACTIONS ON ROBOTICS between 2005-2009, and is currently serving as a Technical Editor of the IEEE/ASME TRANSACTIONS ON MECHATRONICS.